ACS APPLIED MATERIALS & INTERFACES

Research Article

www.acsami.org

Sequence and Temperature Influence on Kinetics of DNA Strand Displacement at Gold Electrode Surfaces

Katarzyna Biala,[†,‡] Ada Sedova,[†] and Gerd-Uwe Flechsig*[,†,‡,§]

[†]Department of Chemistry, University at Albany, SUNY, 1400 Washington Avenue, Albany, New York 12222, United States

[‡]Department of Chemistry, University of Rostock, A.-Einstein-Str. 3a, D-18059 Rostock, Germany

[§]Gensoric GmbH, Schillingallee 68, D-18057 Rostock, Germany

Supporting Information

ABSTRACT: Understanding complex contributions of surface environment to tethered nucleic acid sensing experiments has proven challenging, yet it is important because it is essential for interpretation and calibration of indispensable methods, such as microarrays. We investigate the effects of DNA sequence and solution temperature gradients on the kinetics of strand displacement at heated gold wire electrodes, and at gold disc electrodes in a heated solution. Addition of a terminal double mismatch (toehold) provides a reduction in strand displacement energy barriers sufficient to probe the secondary mechanisms involved in the hybridization process. In four different DNA capture probe sequences (relevant for the identification of genetically modified maize MON810), all but one revealed a high activation energy up to 200 kJ/mol during hybridization, that we attribute to displacement of protective strands by capture probes. Protective strands contain 4 to 5 mismatches to ease their displacement by the surface-confined probes at the gold electrodes. A low activation energy (30 kJ/mol) was observed for the sequence whose protective strand contained a toehold and one central mismatch, its kinetic curves displayed significantly different shapes, and we observed a reduced maximum signal intensity as compared to other sequences. These findings point to potential sequence-related contributions to oligonucleotide diffusion influencing kinetics. Additionally, for all sequences studied with heated wire electrodes, we observed a 23 K lower optimal hybridization temperature in comparison with disc electrodes in heated solution, and greatly reduced voltammetric signals after taking into account electrode surface area. We propose that thermodiffusion due to temperature gradients may influence both hybridization and strand displacement kinetics at heated microelectrodes, an explanation supported by computational fluid dynamics. DNA assays with surface-confined capture probes and temperature gradients should not neglect potential influences of thermodiffusion as well as sequence-related effects. Furthermore, studies attempting to characterize surface-tethered environments should consider thermodiffusion if temperature gradients are involved.

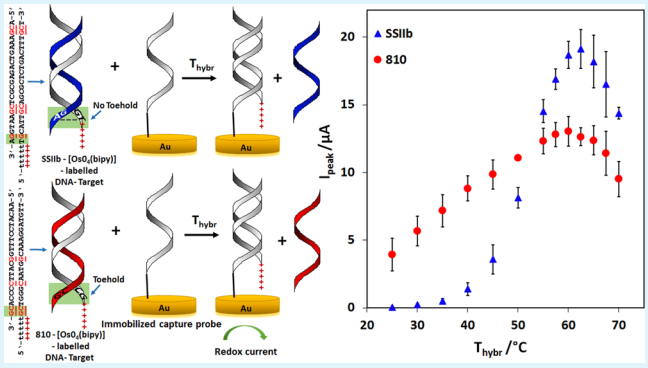

KEYWORDS: *DNA strand displacement, activation energy, gold electrode, osmium tetroxide bipyridine, square-wave voltammetry, thermodiffusion (Soret effect)*

INTRODUCTION

Electrochemical sensors are versatile tools for sequence-specific nucleic acid analysis. Hybridization detection has been performed by means of self-assembled monolayers of capture probes[1−3] and also magnetic beads.[4] Approaches for electrochemical hybridization detection include intercalators such as methylene blue[5] or sandwich assays with an alkaline phosphatase conjugate on biotinylated signaling probes.[6] The different methods of electrochemical hybridization detection have been reviewed several times, for instance by Paleček and Bartosik[7] and Batchelor-McAuley et al.[8] Recently, we have reviewed the literature about temperature effects in electrochemical DNA sensing, revealing that temperature has been gaining increasing attention as a crucial parameter in sequence-specific electrochemical DNA and RNA detection.[9,10] For this purpose, self-assembled monolayers (SAMs) of DNA capture probes are usually immobilized on gold electrodes by means of thiol linkers, sometimes alternatively via direct gold−carbon bonds with diazo-compounds as precursor. Civit et al. considered the thermal stability of such different DNA-linkers on gold electrodes, and found diazo-precursor-based DNA linkers to be the system with superior stability.[11]

Surface plasmon resonance (SPR) spectroscopy has also been used to study temperature effects including melting curves.[12] Cisse et al. discovered a "rule of seven" (subsequently matching base pairs) for predicting thermal stability of dsDNA against

Received: May 21, 2015
Accepted: August 25, 2015
Published: August 25, 2015

DOI: 10.1021/acsami.5b04435
ACS Appl. Mater. Interfaces 2015, 7, 19948−19959

mismatches.[13] Pesciotta et al. studied the influence of mismatch position both in the bulk solution and on the surface. They also found that the dissociation constant K_D for a DNA duplex is significantly larger on the surface than in the bulk solution.[14] Bartlett et al. used surface-enhanced Raman spectroscopy (SERS) to study the effect of electrochemical polarization upon thiol-linked dsDNA denaturation on gold electrodes.[15] Mismatches can be detected this way. A pure electrostatic interaction is apparently not the reason for this kind of melting effect.[16] Molecular beacons (MBs) have also been applied in electrochemical mismatch detection.[17] A dense and well-ordered SAM seems to be crucial for sensors based on MBs.[18] On the other hand, dense probe layers as well as mismatched targets lower the hybridization reaction rate.[19,20]

Recently, Yang et al. used their MB approach for electrochemical melting curve analysis.[21] Before that, several other groups had reported on thermal DNA melting curve analysis with electrochemical detection. Hartwich et al. used osmium labels for the probe and ferrocene labels for the target.[22] The same study revealed that electron transfer rate depends on the distance from the electrode surface, provided that the SAM of dsDNA is well ordered. The single stranded probes yielded the same signal height for the distal osmium label compared with the proximal ferrocene label, suggesting that the SAM of ssDNA probes was not well ordered. Our group used multiple osmium tetroxide bipyridine labels for melting curve analysis. The effects of 1, 2, or 3 mismatches could be discriminated.[23] Nasef et al. used covalent electrochemical ferrocene labels for melting curve analysis,[24] and also methylene blue as an intercalator,[25] as well as fluorescent labels to study DNA melting on gold surfaces.[26] Belozerova et al. used ferrocene,[27] whereas Shen et al. used covalent methylene blue labels.[28]

Covalent labels have a great advantage of being tightly bonded to probe, target or signaling strands. However, labeling during oligonucleotide synthesis leads to diminished yield and increased costs. The complex $[OsO_4(bipy)]$ can be utilized as a covalent DNA-label.[29] The osmium(VIII) reagent reacts readily with nucleic acids[30] in a "click-reaction" under oxidation of the C−C-double bond in the pyrimidine rings forming stable diesters of osmic(VI) acid. Both single-stranded oligonucleotides and PCR products can be labeled this way[31,32] leading to high and reversible voltammetric signals;[30] this method can also be used in hybridization assays with peptide nucleic acids.[33]

Intact double-stranded DNA does not react with $[OsO_4(bipy)]$, while a single strand, thoroughly modified with $[OsO_4(bipy)]$ at all pyrimidine bases, cannot hybridize with its complementary strand. The complex can thus be used to explore the structure of nucleic acids including single base mismatches.[34,35] These properties were also exploited when protective strands were introduced to protect a certain recognition site within the target strand.[31,36] We previously investigated model oligonucleotides from 4 different sequences relevant to genetically modified maize MON810 (SSIIb, CRY, 810, ivrp), in order to analyze multiplexed $[OsO_4(bipy)]$-labeling and hybridization on gold electrodes.[37] Subsequently, we were able to detect less than 0.9% of maize MON810 in real flour samples[38] using these labeling and hybridization protocols for asymmetric PCR products. In these two studies, the hybridization step with gold disk electrodes had been carried out at 40 or 50 °C bulk hybridization solution temperature. Otherwise, temperature effects on hybridization detection with gold electrodes, using these sequences, have not been investigated. There are only a few other studies about acceleration of the hybridization process on electrochemical DNA sensors. Liu et al. proposed "acoustic micromixing," leading to 5-fold acceleration.[39] Sosnowski et al. applied constant electrical fields on agarose-streptavidin modified electrode arrays coupled with optical hybridization detection.[40]

Ten years ago, we introduced a probe-SAM-modified heated gold wire electrode to perform DNA hybridization at desired elevated temperatures. We found a 140-fold increase of the hybridization signals at higher electrode temperatures.[41] In earlier studies, such directly heated electrodes had been found advantageous for heavy metal[42,43] and DNA stripping analysis.[44] We also performed DNA melting curve analysis by means of heated electrodes.[23] If mass transport can be identified as the rate-limiting step, as is the case for fast reactions like reductive metal deposition, the enhancement factor is typically 10-fold.[42,43] Otherwise, if kinetically sluggish processes like reduction of arsenic(V) or adsorption of dsDNA at carbon electrodes are rate determining, improvement of electrochemical signals of 30-fold and more were observed if elevated electrode temperatures were applied.[44] Fundamental and basic studies of heated electrodes have been reviewed several times.[45−48] Our heating device allows direct electrical heating of a broad variety of electrode designs.[49]

The behavior of short oligonucleotides tethered to surfaces has been found to be difficult to accurately characterize and explain, especially for single-stranded molecules.[50−53] Deconvolution of the multifarious contributions from electrostatics, excluded volume, crowding, and surface-molecule interactions to surface-regime kinetics has been challenging both theoretically and experimentally, yet these effects have been shown to result in dramatic differences as compared to the solution setting.[50−52] Surface-tethered assays, such as microarrays, have become an essential biotechnology used in numerous applications from pharmaceutical development, to cancer diagnostics, to forensics; however, accuracy and reliability of these methods are still proving difficult to optimize, due in large part to a lack of thorough understanding of exact details of the biophysical properties underlying these processes.[51] For a solution-based experiment such as ours, the influence of bulk diffusion of the molecules of interest as well as the fluid dynamics of the solution both around the electrode and in more distal regions of the bulk volume must also be considered as a potential influence on the assay.

Thermodiffusion, or the Soret effect, is the motion of molecules in a specific direction in response to a temperature gradient.[54−56] Frequently, more massive molecules will move to the colder region, however, influences of molecular interactions and temperature ranges have been found to occasionally result in reversal of direction of motion.[57,58] While this effect has been used in industry for over a century,[54] it has only been described empirically, in varying levels of detail, and its molecular origins have not been explained, even being referred to as "one of the unsolved puzzles in physical chemistry."[56] The linear-response theory, nonequilibrium thermodynamics description of thermodiffusion is based on the Onsager relations and involves empirical coefficients which must be measured experimentally or estimated.[55] This model assumes the absence of any free convection, and assumes a steady state: considered to occur at the time when the mass transfer of the solute due to the thermophoretic force is balanced by the opposing response of diffusion due to the concentration gradient set up by the thermophoresis.[54−56] The Soret coefficient is then the ratio of the diffusion due to thermophoresis to the diffusion due to the resulting concentration gradient. Originally, the concentration on the depleted side and the concentration on the enriched side were measured, and the temperature difference between hot and

DOI: 10.1021/acsami.5b04435
ACS Appl. Mater. Interfaces 2015, 7, 19948−19959

cold was used to apply an empirical formula to obtain the Soret coefficient.[54] When convection is involved, a detailed mathematical description results in a system of coupled differential equations which are much more difficult to solve than those provided by the Onsager relations.[59] While the influence of the Soret effect had been traditionally assumed to be negligible in most solution experiments, research over the past few decades has shown that this effect can play a very significant role in small-volume settings, and seems to have a particular influence on nucleic acids in solution.[57,58,60−62]

In this work, we report dramatic temperature effects observed during hybridization detection of different DNA oligonucleotide sequences. This hybridization step on gold electrodes was coupled with a strand displacement. Due to the use of [OsO_4(bipy)], we applied protective strands that have the same sequence as the capture probes, except for a few mismatches that we have introduced to foster the strand displacement reaction. Our findings reveal that such strand displacements, in many cases, require very high activation energy. For a particular sequence with a double terminal mismatch (toehold), however, the activation energy was found to be greatly reduced, and enabled a glance into processes secondary to the strand displacement step, such as diffusive phenomena. This finding suggests an avenue for probing both the surface environment and bulk transport-related diffusion influences on such assays in future studies. Additionally, performing the strand displacement reaction at heated gold-wire electrodes resulted in surprising differences compared to results obtained with gold disk electrodes in a heated bulk hybridization solution. These results can be explained in part by a possible presence of the Soret effect resulting from large temperature gradients in proximity to the heated microelectrode. A computational fluid dynamics analysis supports this interpretation.

EXPERIMENTAL SECTION

Materials. For the experiments described here, we used the same four maize MON810 sequences as earlier reported:[37,38] SSIIb (starch synthase gene IIb of maize) and ivrp (invertase gene of maize) as a positive control for the detection of any maize and probes CRY (existence of the cryIa/b transgene within the sample) and 810 (existence of the transgene at the MON 810 specific insertion locus) for the specific detection of the GM-maize.

Sequence ivrp

Capture probe ivrp:

5′-CACGTGAGAATTTCCGTCTACTCGAGCCT-aaaaaaaaaaaaaa[Dithio]$_3$-3′ (29 + 15a)

Protective strand ivrp:

5′-CA**GC** TGAGAATTTCCGTCTA**G** T**GC** AGCCT-3′ (29)

Target ivrp:

5′-tttttAGGCTCGAGTAGACGGAAATTCTCACGTG-3′ (29 + 5t)

Sequence SSIIb

Capture Probe SSIIb:

5′-AGCAAAGTCAGAGCGCTGCAATGCAaaaaaaaaaaaaaaa-[Dithio]$_3$-3′ (25 + 15a)

Protective strand SSIIb:

5′-A**CG** AAAGTCAGAGCGCT**CG** AATG**G** A-3′ (25)

Target SSIIb:

5′-tttttTGCATTGCAGCGCTCTGACTTTGCT-3′ (25 + 5t)

Sequence CRY

Capture Probe CRY:

5′-AGATACCAAGCGGCCATGGACAACAAaaaaaaaaaaaaaaa-[Dithio]$_3$-3′ (26 + 15a)

Protective strand CRY:

5′-AGATA**G** CAAGCGGCCATG**C** A**G** AA**G** AA-3′ (26)

Target CRY:

5′-tttttTTGTTGTCCATGGCCGCTTGGTATCT-3′ (26 + 5t)

Sequence 810

Capture Probe 810:

5′-AACATCCTTTGCCATTGCCCAGCaaaaaaaaaaaaaaa-[Dithio]$_3$-3′ (23 + 15a)

Protective strand 810:

5′-AACATCCTTTG**G** CATT**C** CCCA**CG** −3′ (23)

Target 810:

5′-tttttGCTGGGCAATGGCAAAGGATGTT-3′ (23 + 5t)

Melting temperatures were calculated, for reference, by means of OligoAnalyzer 3.1 (PrimerQuest program, IDT, Coralville, USA), resulting in the following values for ivrp, SSIIb, CRY and 810 capture probe-target duplexes: 76.6 °C, 77.5 °C, 76.5 °C, and 74.5 °C, respectively. 2,2′-Bipyridine was purchased from Merck and osmium tetroxide was obtained as a 2% aqueous solution from Fluka. The Tris-buffer containing 10 mM tris(hydroxymethyl)-aminomethane and 0.5 M Na_2SO_4 was adjusted to pH 7.5 using sulfuric acid. All DNA oligonucleotides were delivered by biomers.net GmbH, Germany. The probe strands contained 15 adenine bases as a spacer to allow high hybridization efficiency on the electrode surface. All electrochemical measurements were performed in a 3-electrode system using an Autolab PGSTAT 12, (Ecochemie, The Netherlands). The reference electrode was an Ag/AgCl (3 M KCl) electrode (Metrohm, Switzerland) and the counter electrode was a glassy carbon rod (Metrohm). A modified gold disc electrode (diameter 2 mm, Metrohm) and an in-house-made heatable (25 μm diameter, 5 mm length) gold-wire electrode[41] were used as the working electrodes. The bulk solution temperature during the hybridization process on the gold disc electrodes was controlled by means of a thermostat (Huber). The gold microwire electrode was heated directly by means of an HF ThermaLab heating generator (Gensoric GmbH, Rostock, Germany).

Target and electrode preparation. The DNA-targets were labeled with [OsO_4(bipy)] by means of protective strands.[31] In the first step, 25 μL unlabeled DNA-Target solution and 25 μL protective strand solution (each 100 μM in Tris-buffer) were mixed together and left for 2 h at room temperature to allow hybridization. Then 12.5 μL of 10 mM [OsO_4(bipy)] were added to label the five unprotected 5′-terminal thymine bases and left again for 2 h at room temperature. This way, the recognition site of the signaling strand remained unmodified. To remove the excess of [OsO_4(bipy)], the solution was placed into a dialysis cell (Slide-A-Lyser Mini Dialysis Units, USA, Rockford). Dialysis was performed against Tris-buffer at first for 1 h and again after refreshing the buffer overnight at 4 °C. According to earlier reports, this procedure was sufficient to remove all excess of [OsO_4(bipy)].[63] After the dialysis, the solution containing the [OsO_4(bipy)]-labeled target was used at the given concentration for the hybridization experiments. Before each measurement, the gold disc electrode was polished using corundum 0.3 μm (Buehler GmbH, Germany) and thoroughly rinsed with ultrapure water. Ultrapure water was prepared by means of an SG Water system (2005, SG Water GmbH, Germany, now Evoqua LLC); 18 MΩ*cm, TOC better than 2 ppb. A new gold wire electrode was prepared prior to each probe DNA immobilization. The gold wires were cleaned by electrical heating to red glowing in air. After the first cleaning step, both the gold disk and the gold-wire electrodes were cleaned electrochemically by using cyclic voltammetry (25 scans, − 0.3 to 1.7 V, scan rate 100 mV/s) in 0.5 M sulfuric acid. After rinsing the electrodes with water, they were then dried under a stream of nitrogen. In the next step, a probe solution (30 μM in Tris-buffer) was placed onto the cleaned electrode surface in order to form the capture probe SAM. After 16 h at room temperature in a water-saturated atmosphere, the electrodes were immersed in 1 mM aqueous 6-mercapto-1-hexanol solution for 1 h to fill the gaps between the probes, thus minimizing capacitive currents and preventing any nonspecific DNA-adsorption on the electrode surface. After rinsing the ssDNA-SAM-modified-electrodes with water, they were used for hybridization experiments with the target strands.

Hybridization step and measurements. For the hybridization, the gold disc electrode was dipped for 15 min into a heated buffer solution containing the labeled DNA target. The bulk solution temperature during the hybridization process on the gold disc electrodes was controlled by means of a thermostat and a water jacketed glass cell.

DOI: 10.1021/acsami.5b04435
ACS Appl. Mater. Interfaces 2015, 7, 19948−19959

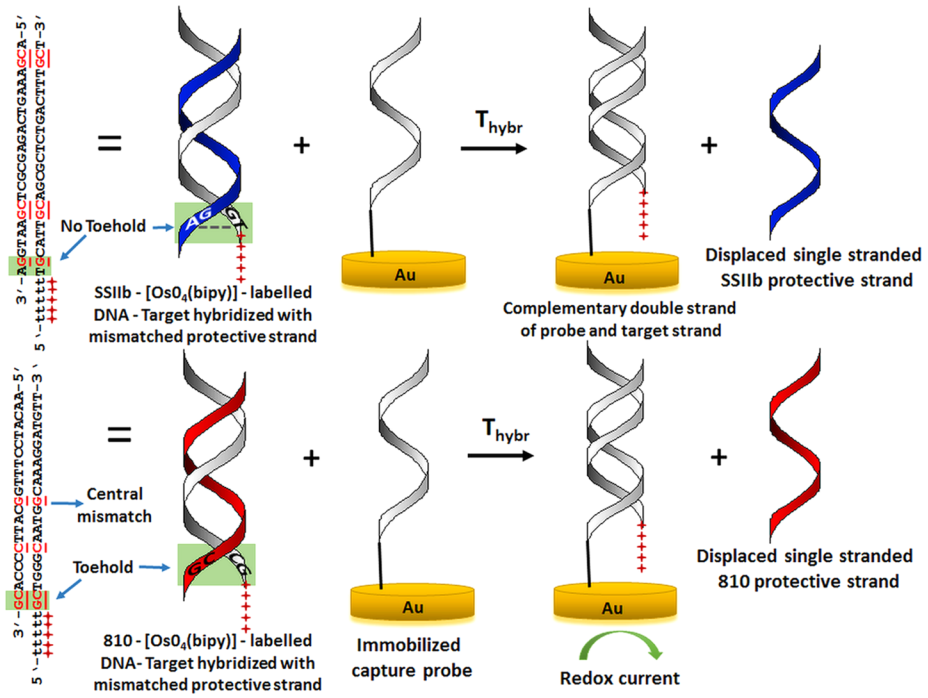

Figure 1. DNA detection procedure by means of protective strands and labeling with [OsO_4(bipy)]. The protective strand, which is partially complementary, hybridizes with a single stranded target sequence. After the hybridization, [OsO_4(bipy)] is added. [OsO_4(bipy)] reacts with the five terminal, unprotected thymine bases. The labeled target is detected using a complementary capture probe, which is immobilized on a gold surface. The electrochemical current increases after the hybridization of target with the probe.

For the hybridization at the directly heated gold wire electrodes, the electrode was dipped into an 8 °C target solution, for 15 min as well, while the gold wire was directly heated with an AC heating current by means of the ThermaLab heating generator. Circuitry, potentiometric temperature calibration of the electrode and an experimental setup for electrode heating have been described earlier.[49] Note that replicating the exact conditions as those found in the disc electrode setting is impossible for our wire electrode system, as the material surrounding the wire electrode cannot withstand immersion in solutions of temperatures much greater than 50 °C. After hybridization the electrode was rinsed with Tris-buffer and then dipped into an electrochemical cell in order to perform measurements. All electrochemical measurements were performed at room temperature in the Tris-buffer using square-wave voltammetry (SWV) with the following parameters: start potential −0.55 V, end potential 0 V, amplitude 40 mV, frequency 200 Hz. After the voltammetric measurements, the gold disc electrode was immersed into 50 °C water for 60 s, while the gold wire electrode was also immersed into water for 60 s, but electrically heated to 41 °C to allow dehybridization and regeneration of the capture-probe SAM. After detecting the dehybridization signal, the electrodes were used again for another hybridization reaction at another temperature. The peak-shaped voltammetric signals were smoothed according to Savitzky and Golay, and baseline-corrected using the GPES 4.9 software.

Simulation of heat transfer, temperature distribution and convection. For preliminary calculations, the classical two-dimensional free convection model of two temperature plates separated by an insulating layer, using a characteristic temperature gradient and size scale for our system, was considered analytically to derive an approximate estimate of expected average temperature and momentum boundaries and confirm the assumption of a laminar regime. For this model, it is possible to analytically estimate the Reynolds number, the Raleigh number, the Prandtl number, the momentum and temperature boundary, and the average order of magnitude of the velocity due to buoyancy forces, with and without consideration of the effects of viscosity. For the size scale and temperature gradient in the heated wire electrode system, as well as for the gold disc electrode in heated bulk solution, these calculations showed a regime well in the laminar region, with temperature and momentum boundaries of about 0.8−0.5 mm, and estimated an average velocity on the order of magnitude of 1 to 10 mm/s.

Using the conjugate heat transfer, laminar flow portion of the heat transfer module of COMSOL Multiphysics version 5.1 (COMSOL Inc.), several models of the experimental systems were created for simulation. In all models, temperature dependent functions for density, dynamic viscosity, and heat capacity at constant pressure were used for water, and constants were used for the gold surfaces. The gold wire electrodes were modeled using the conductive thin layer boundary setting, and the gold disc was modeled as a solid. The sheath around the gold disc electrode was included, with the appropriate values of thermodynamic constants specific to peek. For the wire, a boundary heat source was set to 0.8 W, which created a temperature at the wire surface of 313.2 K.

For the three-dimensional model of the wire, the entire bulk system was initially calculated (hereafter referred to as coarse-grained model), using a symmetric boundary cross-section to decrease computational time. These calculations, while considering the overall scale of the entire experiment, were not fine-grained enough to capture fluid dynamics in the smaller region immediately around the wire. However, they are used to justify the settings used in the detailed model, which considers a smaller region around the wire, in order to use a more detailed mesh and achieve corrected values for velocity and temperature.

For the detailed calculations, the 5 mm wire surrounded by a 3 mm × 3 mm × 8 mm box of fluid, cooled to 283.15 K on all exterior boundaries except the top boundary, was simulated. The top boundary was set to a temperature of 288.15 K, according to the effects of a layer of air on top of the bulk model, simulated by a conductive boundary layer. The actual model created was half of this system, with an added symmetry boundary at the radial cross section of the middle of the wire, to reduce computational time. A graded mesh was used which increased in size from 12 μm at the wire surface, to 200 μm in the bulk fluid, at the appropriate regions for fluid dynamics and heat transfer. Both steady-state calculations and time dependent calculations with time steps of 0.5 s ranging from 0.5 to 10 s were performed.

Additionally, an axisymmetric model of the disc electrode in a heated bulk solution was simulated, also using the conjugate heat transfer multiphysics node, and again considering the entire bulk volume as a

DOI: 10.1021/acsami.5b04435
ACS Appl. Mater. Interfaces 2015, 7, 19948−19959

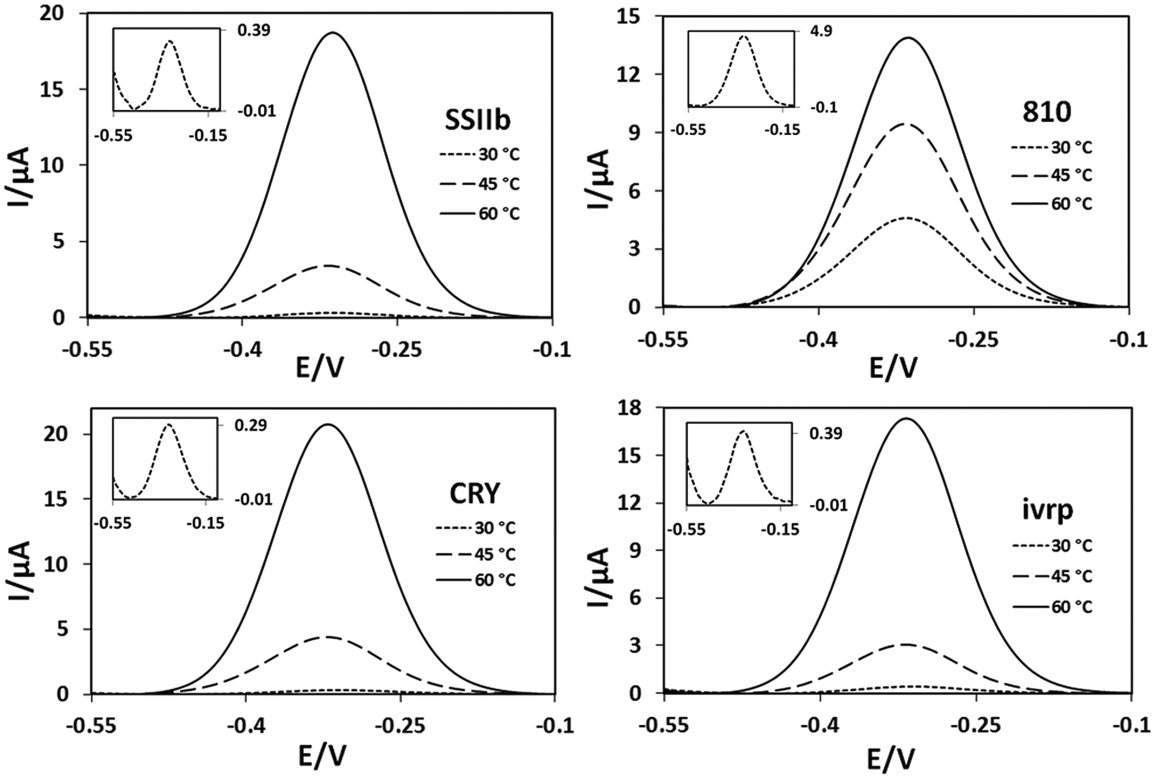

Figure 2. Square-wave voltammetric response of 4 different target strands labeled with [OsO_4(bipy)] obtained at gold disc electrodes in Tris-buffer after 15 min of hybridization with immobilized capture probes at 0.2 μM target concentration at 3 different hybridization temperatures. SWV conditions: frequency 200 Hz; amplitude 40 mV. During the hybridization step, the solution was stirred with a magnetic stirrer. The insets show magnified SWV peaks obtained at 30 °C hybridization temperature. Signals were smoothed using Savitzky and Golay followed by baseline correction.

coarse-grained model, and then a smaller region with the same dimensions as used in the detailed model of the wire. Steady-state and time-dependent calculations were performed for the coarse-grained model, and time-dependent only for the detailed model. Further simulation details such as mesh size and parameters can be found in the Supporting Information.

RESULTS AND DISCUSSION

Gold disk electrodes in a heated hybridization solution. Figure 1 displays the detection procedure, including the location of mismatches, the toehold, and the osmium label. Figures 2 and 3 demonstrate an extreme effect of bulk solution temperature during the 15 min hybridization step. In case of sequence SSIIb, a 319-fold increase of hybridization signals was observed when going from 25 to 62.5 °C bulk hybridization solution temperature. Also CRY and ivrp sequences revealed a similarly dramatic temperature behavior. The according Arrhenius plots (Figure 4 and Table 1) were calculated for the exponential first parts seen in Figure 3, and indicate very high formal activation energies of 123.8, 130.8, and 150.9 kJ/mol for sequences ivrp, CRY, and SSIIb, respectively. Even the pre-exponential factors are very high ranging between 6.1×10^{20} and 1.85×10^{25} μA. The sequence 810 stands out remarkably, its activation energy being only 29.7 kJ/mol and the pre-exponential factor 7.2×10^{5} μA. An error estimation for these parameters is provided in the SI. Literature findings confirm that such high values for activation energies are not uncommon for strand displacement reactions. Furthermore, a so-called toehold region can greatly accelerate this process.[64] A 2-nucleotide toehold containing only G or C, as found for sequence 810 and its protective strand, can accelerate the displacement rate by factor 1000.[65] The dramatic difference in pre-exponential factors is even more astonishing. The large numbers can be attributed to the measure (peak current in A) that we have chosen as a representative for the reaction constant. Taking into account the unit prefix (10^{-6}), the Faraday constant (96,485 C/mol) and the 10 transferred electrons, the pre-exponential factor values would be lowered by 12 orders of magnitude. However, in square-wave voltammetry, the peak current is proportional to the transferred charge, but the latter cannot be calculated by simple integration of the peak area. Linear sweep voltammetry or chronocoulometry would be needed to obtain information about the transferred charge. What is probably more important here, is the huge difference in pre-exponential factors. As pre-exponential factors (a measure for collision frequency and steric conditions) for similar reactions with comparable reactants are relatively equal, the observed difference indicates that another reaction step is rate limiting for 810, probably surface diffusion instead of strand displacement. The activation energy of 29 kJ/mol is relatively high for bulk diffusion in water, but might be indicative for surface diffusion. In other words, the very large difference in pre-exponential factors suggests that strand displacement is not the rate-limiting step for 810 sequence.

Assuming that the rate-limiting kinetics for 810 are not strand displacement, the experimental results for this sequence can be analyzed as reporting on the secondary processes involved in these reactions. For both the disc electrode and the wire electrode, the shape of the kinetic curves for 810 are not sigmoidal, indicating that the reaction cannot be modeled by a single exponential, and does not have a single rate-limiting step. This indicates that certain aspects of the various bulk transport and surface-environment factors may contribute equally to the

DOI: 10.1021/acsami.5b04435
ACS Appl. Mater. Interfaces 2015, 7, 19948−19959

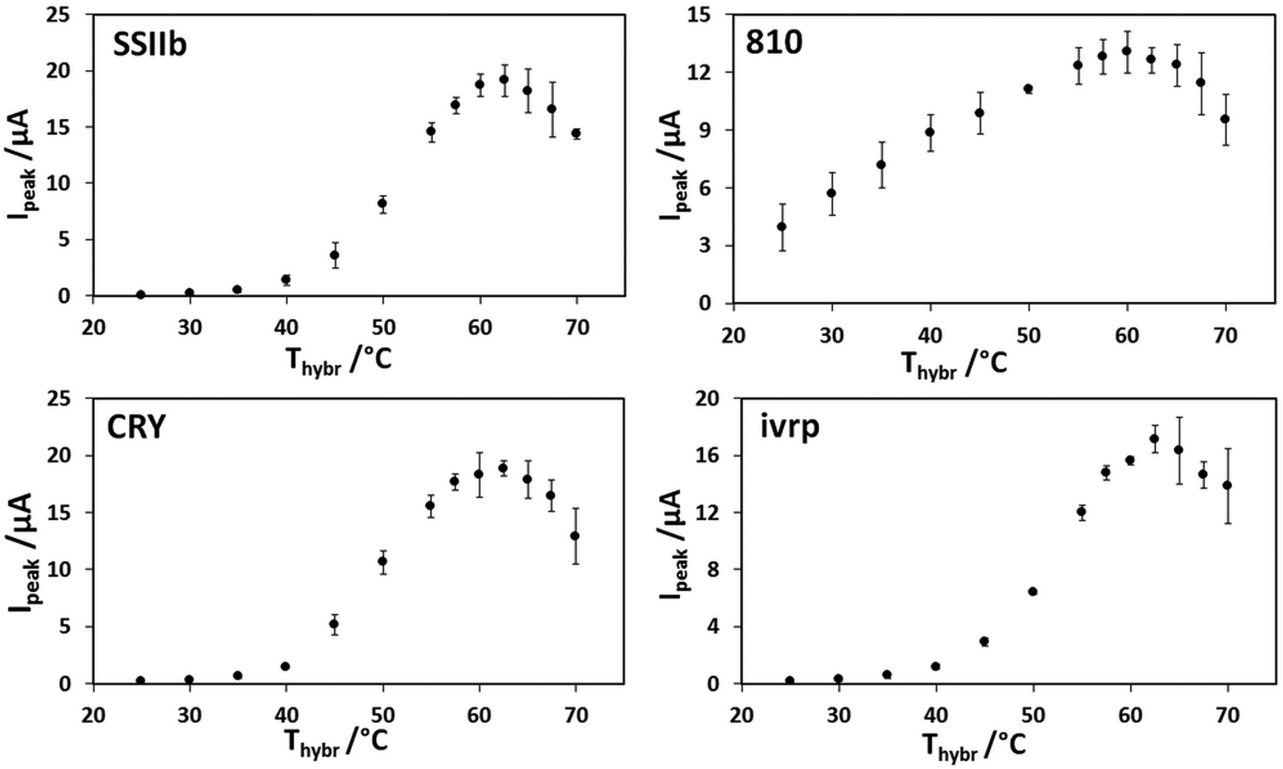

Figure 3. Influence of hybridization temperature on square-wave voltammetric signals of 4 different target sequences with their capture probes immobilized on gold disc electrodes in Tris-buffer after 15 min of hybridization under magnetic stirring in 0.2 μM DNA target. T_{hybr} represents the temperature of the target solution during the hybridization step. SWV conditions and data processing were the same as in Figure 2. The error bars indicate standard deviations of three independent repetitive measurement series, each obtained with a newly prepared probe SAM.

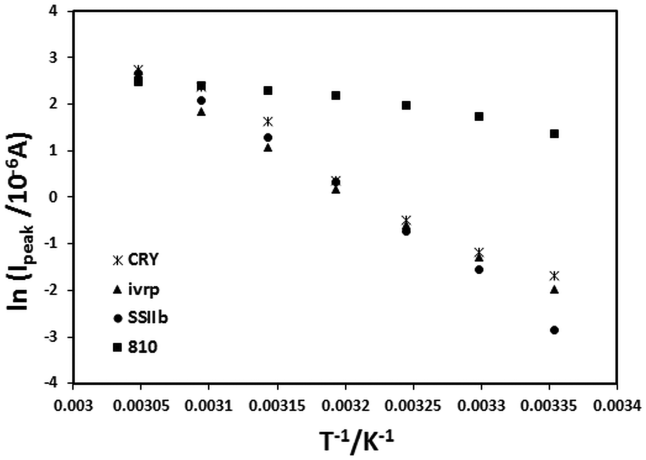

Figure 4. Arrhenius plots for the hybridization data sets obtained with gold disk electrodes as depicted in Figure 3.

Table 1. Activation Energies and Pre-exponential Factors from the Arrhenius Plots Depicted in Figure 4

maize sequence	E_a [kJ/mol]	A [μA]
SSIIb	150.9	1.85×10^{25}
CRY	130.8	1.61×10^{22}
ivrp	123.8	6.07×10^{20}
810	29.72	7.22×10^{5}

reaction. Furthermore, for the disc experiment, the maximum signal is lower than for the maximum signal observed for the other sequences (the same is true for the wire setting also, but error bars preclude making conclusions here). This indicates that a sequence-related effect on some aspect of the secondary processes works to decrease overall hybridization rates. One possibility is that the combined presence of the toehold and the heavy osmium moiety on the same end of the strand increases friction and slows diffusion rates either in the bulk solution, at the electrode surface, or both. The second lowest signal is observed for SSIIb, which has a single mismatch at the base second from the terminal base, thus this sequence may also experience similar, though reduced, drag forces.

Since we were using a 3′-$(dA)_{15}$-spacer for all our capture probes and a 5′-$(dT)_5$-end for all our targets, our results also suggest that [OsO_4(bipy)]-labeled thymines cannot act as a toehold. This is not completely surprising, as Paleček et al.[29] have been reporting for some 30 years that [OsO_4(bipy)]-labeled thymines prevent a single strand from further hybridization. This was the reason why we introduced the protective strands in the first place 10 years ago, in order to perform hybridization with partially [OsO_4(bipy)]-labeled strands at gold electrodes.[66] Another possible factor that could lead to accelerated displacement of the 810 protective strand could be that one of the protective strand mismatches is located exactly in the middle of the sequence. Internal mismatches destabilize a DNA duplex significantly more, in comparison to near-terminal and terminal mismatches.[14,67]

Heated gold wire electrodes. The sequences SSIIb and 810 were also studied at heated gold microwire electrodes as depicted in Figure 5 (see Table 2 for activation energies and pre-exponential factors). The highest voltammetric hybridization signals at the gold microwire were about 150-fold smaller compared with the gold disk electrode. This cannot be fully explained by the different surface areas (factor 8), even in

DOI: 10.1021/acsami.5b04435
ACS Appl. Mater. Interfaces 2015, 7, 19948−19959

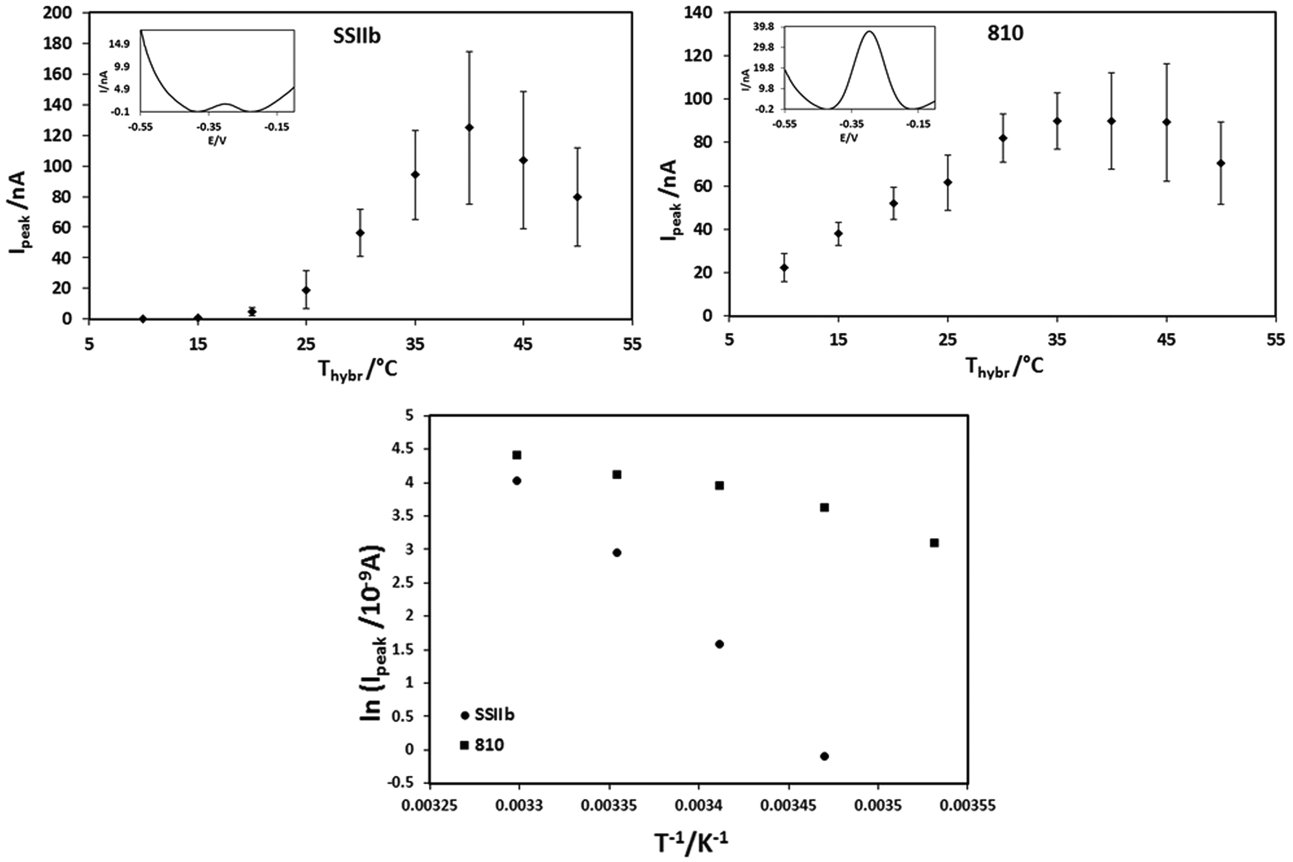

Figure 5. Influence of gold microwire electrode temperature on square-wave voltammetric signals of the target sequences SSIIb and 810 (0.2 μM) with their immobilized capture probes after 15 min of hybridization in Tris-buffer. SWV conditions and data processing were the same as in Figure 2. The error bars indicate standard deviations of three independent repetitive measurement series, each obtained with a newly prepared probe SAM. The insets display representative SWV signals obtained after hybridization at 15 °C electrode temperature. Signals were smoothed using Savitzky and Golay followed by baseline correction. Also shown are the linear parts of the according Arrhenius plots.

Table 2. Activation Energies and Pre-exponential Factors from the Arrhenius Plots Depicted in Figure 5

maize sequence	E_a [kJ/mol]	A [μA]
SSIIb	200.0	1.86×10^{33}
810	44.2	3.55×10^{6}

combination with a different probe surface coverage (factor 3), that we had observed earlier.[41] Otherwise, we found a basically similar thermal hybridization behavior. The activation energies were now significantly higher with 200 and 44.2 kJ/mol for the sequences SSIIb and 810, respectively. Both the great difference in activation parameters and the general trend for both sequences were comparable to hybridization at the gold disk electrode. However, the optimal hybridization temperatures at the heated gold wire electrode were much lower in comparison with hybridization at the gold disk in the heated bulk solution. This corresponds with findings that we had reported earlier:[23,41] Our first report on DNA hybridization at heated gold wire electrodes revealed dramatic temperature dependence. In that study we used 80 nM ferrocene labeled targets that yielded small AC voltammetric signals up to 400 pA after 4 min hybridization.[41] The covalent osmium labels that we used in the present study delivered 10-fold more electrons than the single ferrocene label. Also, the measurements with a heated gold microwire electrode in that early study yielded a low voltammetric signal level. Later we found no significant difference in optimal hybridization temperature when comparing a rotating gold disk electrode in a heated solution with an indirectly heated gold disk electrode.[68] In another study, electrochemical DNA melting curves obtained with capture probes immobilized on gold disk electrodes indicated significant differences in melting temperature (5 to 8 K) depending on whether the entire bulk solution or only the gold disk electrode was heated.[23] Here in this present study, in case of the maize sequences SSIIb and 810, the difference in optimum hybridization temperature obtained at different electrode types was very large. For sequence 810, this value was lowered by 25 K, and for SSIIb, we found a 22 K decrease. A major difference to our earlier DNA melting study[23] was that we did not work under equilibrium conditions, i.e. this time we hybridized for only 15 min instead of 16 h. This might be one reason why in the earlier study the decrease of melting temperature was only 8 K when going from heated bulk solution to heated gold wire electrode. That was in accordance with all the other reports on thermodynamic stability of DNA duplexes.

Applicable in our current study, however, are nonequilibrium conditions, where kinetic parameters such as the mass transport toward and from the electrode surface control the signal height. Thermal convection that occurs around a heated electrode, can be very intense compared with magnetic stirring at the disk electrodes.[69] In our case, intense convective mass transport also facilitates the removal of displaced protective strands, and thus, accelerates the strand displacement process. Moreover, several studies have revealed dramatic effects of thermodiffusion

DOI: 10.1021/acsami.5b04435
ACS Appl. Mater. Interfaces 2015, 7, 19948−19959

(thermophoresis, Soret effect) upon mass transport in a temperature gradient,[70] particularly in the case of larger molecules such as DNA.[62] Very large temperature gradients can indeed be found around a heated microwire[71] due to cylindrical heat distribution, but not at a disk electrode inside a heated bulk hybridization solution. Because of planar heat distribution at the indirectly heated gold disk electrode considered above,[23] the temperature gradients are expected to be lower. Braun et al. found that the Soret effect for DNA molecules in aqueous electrolyte solution depends on DNA size, temperature, ionic strength (Debye length),[62] and type of electrolyte, because it is coupled with the Seebeck effect.[58,72] Accordingly, for the DNA strands and hybridization conditions studied in this work, the Soret coefficient is expected to be positive. That means, both the protected DNA target strands and the released protective strands tend to flee from the heated wire electrode into the cold bulk solution. For the protective strands this movement points into the same direction as the diffusion caused by the concentration gradient. For the target strands, however, thermophoresis and diffusion point into opposite directions. We think that together, this will facilitate the strand displacement, but lead to overall small signals. The Soret effect has been seen as a negligible factor when considering the emf of nonisothermal cells comprising heated electrodes.[46] Mass transport of large analyte molecules with or without electrochemical polarization, however, seems to be greatly influenced, especially if coupled with thermal convection. This will require closer attention in future studies.

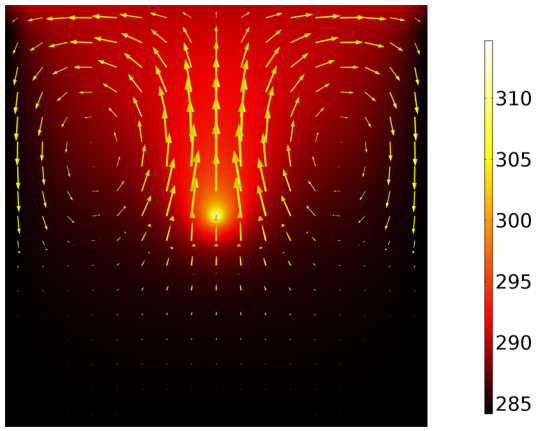

Figure 6. Temperature contour plot (K) overlaid with velocity field for stationary solution, detailed model of heated wire electrode. Arrow size represents velocity magnitude. The size of the slice is 3 mm by 3 mm.

Simulation results. For the wire electrode models, for the coarse-grained model, temperature gradients did not reach steady-state values by 10 s, although they were similar (see Supporting Information). Differences were found in the regions of the bulk closer to the air interface and showed slightly higher values at steady state. Velocity values were close for steady state and 10 s, however, their distribution was slightly different as can be seen by isosurface plots in the Supporting Information. For the detailed model, temperature gradients in the local region were found to reach steady state values in 10 s, and velocity profiles did not reach the exact steady state values by 10 s, although they approached closely. Velocities at steady state were reduced in magnitude, but streamline directions and overall flow was very similar. The coarse-grained model shows that the majority of the solution can be found at a temperature of 283−284 K, with a region approximately 1 mm by 2.75 mm by

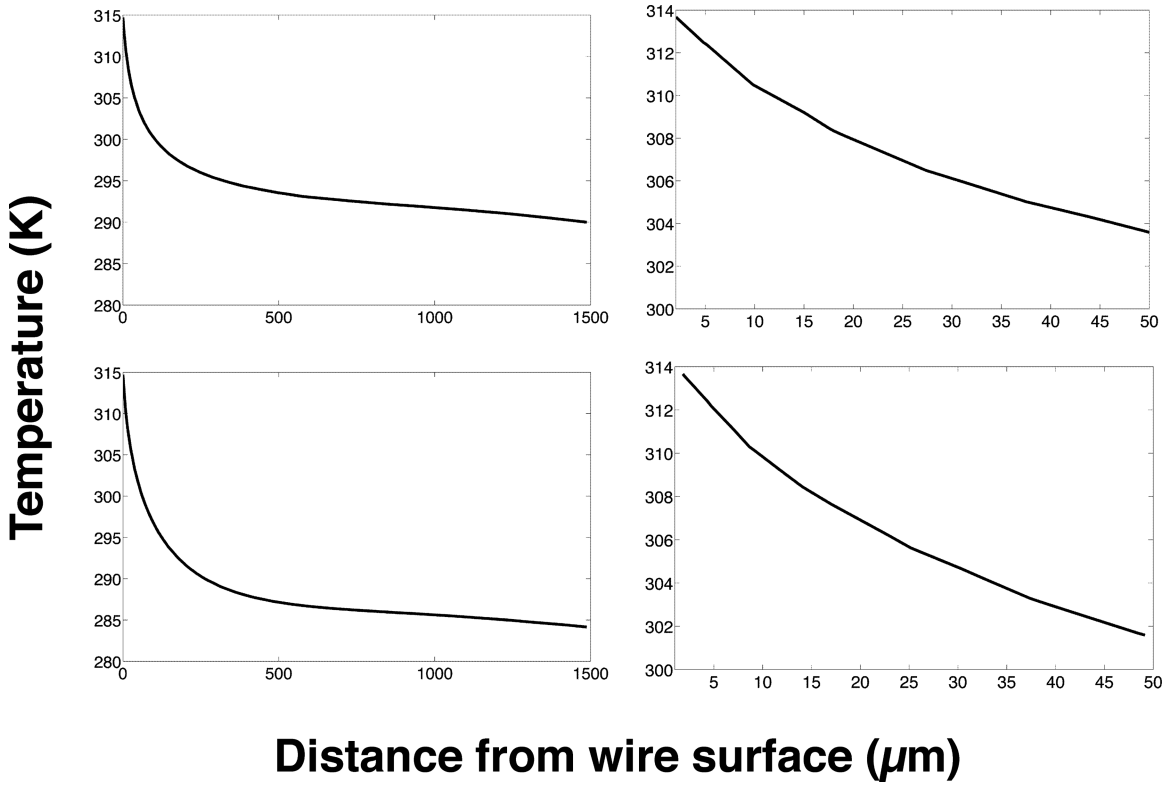

Figure 7. Temperature profiles for stationary solution, heated wire electrode, detailed model, along radial line in *y*-direction (top) and *x*-direction (bottom) of a cross-sectional slice at 0.5 mm from wire center. The cross-sectional slice is the same as visualized in Figure 6. Right hand side is a close-up of the left-hand side.

DOI: 10.1021/acsami.5b04435
ACS Appl. Mater. Interfaces 2015, 7, 19948−19959

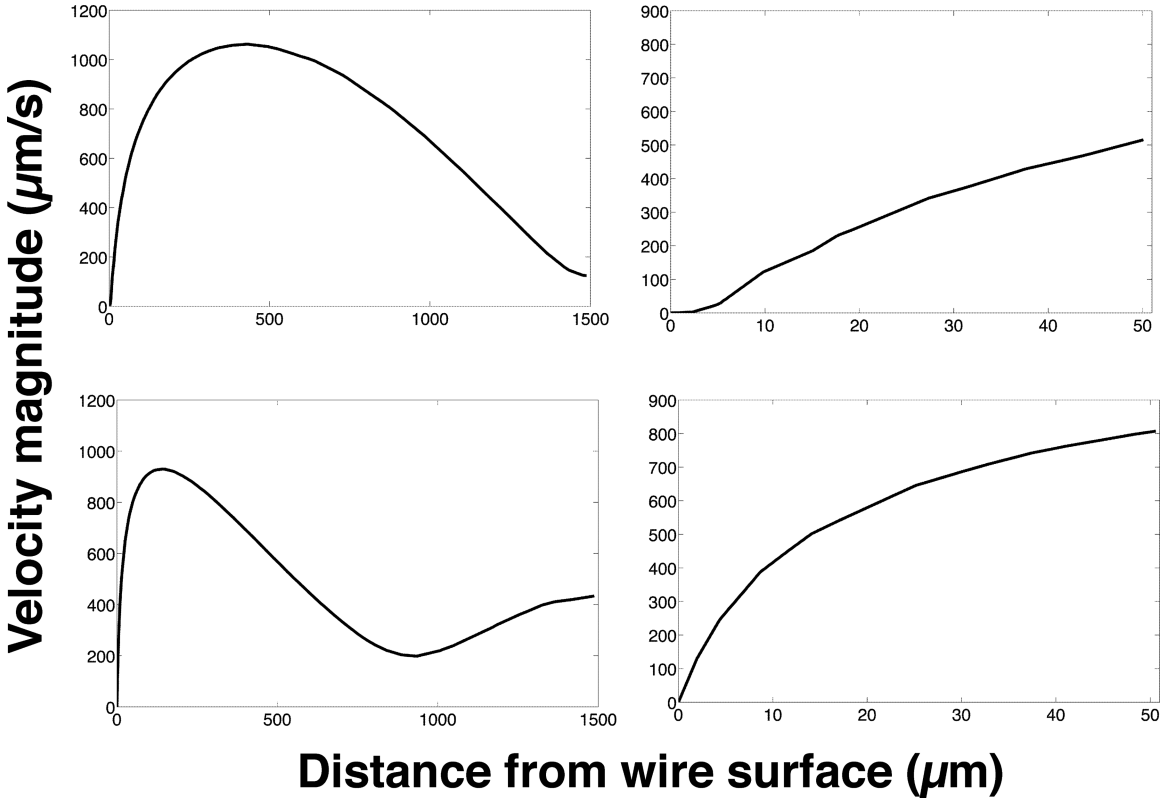

Figure 8. Velocity magnitude profiles, for stationary solution, heated wire electrode, detailed model, along radial line in *y*-direction (top) and *x*-direction (bottom) of a cross-sectional slice at 0.5 mm from wire center. The cross-sectional slice is the same as visualized in Figure 6. Right hand side is a close-up of the left-hand side.

3 mm containing higher temperatures, ranging from 285 to 314 K. Velocity profiles in the coarse-grained model showed significant convective circulation, and velocity magnitudes followed a similar pattern as temperature, but with additional regions of varying circulating velocities found in regions further away from the wire. Temperature and velocity profiles for time dependent and steady state analyses can be seen as 2D colormap slices, 2D contour maps, and 3D isosurface plots in the Supporting Information. Maximum velocities for the coarse-grained wire model were found to be around 2.5 mm/s, however, these values are not extremely accurate as the grid size and velocity finite element order was large due to computational cost limitations.

The detailed wire electrode model finds corrections to the calculated temperatures and velocities near the wire. Figure 6 shows a contour plot of steady state values for temperature over a cross-sectional slice found 0.5 mm from the wire center, which is the symmetry boundary. The image shows the entire width and height of the detailed model, which is 3 mm × 3 mm. An overlay of velocity field lines shown as arrows scaled according to velocity magnitude, for this same cut-plane, is also shown. Figure 7 displays temperature and velocity as a function of distance from the electrode for the same cut-plane, traveling radially along the y- and *x*-directions, also for the steady state. Temperature gradients are steeper in the *x*-direction, and reach values close to the cooled bulk within 500 μm of the wire. For both directions, a temperature difference of about 3.5 K can be found over the first 10 μm. The Supporting Information also shows temperature and velocity profiles for time dependent and steady-state computations in the detailed setting.

Figure 8 shows the same radial line plots for velocity magnitude over the same cut-plane as for the temperature profiles in Figure 7. Maximum velocity in the region was found to be 1.08 mm/s, and is located above the wire. A lower velocity region, found immediately surrounding the wire, is found in this detailed model, with velocity magnitudes ranging from about 50 μm/s, one μm from the wire surface, to about 400 μm/s, 10 μm from the wire surface. Lower velocities are found in the region directly above the wire, as can be seen from the plots of the *y*-direction radial profiles. While this finding is similar to previous results[71] and velocity profile estimations[73] noting an apparent "quiescent solution layer" of ca. 8 μm, it is difficult to know exactly what velocity designates a purely diffusive regime. Translational self-diffusion of single-stranded and duplex DNA of length 12−40 bp, converted to a one-dimensional value in order to compare to velocity values, is of the order 10 μm/s, with estimated values ranging from 7 to 13 μm/s.[74] Concentration-driven diffusion of DNA oligonucleotides was also estimated to be around 10 μm/s when considered as a one-dimension value.[62] Thus, the diffusive regime may only be found in a region less than 5 μm away from the wire surface, where the velocity magnitude stays below 50 μm/s, and this is still much greater than most estimates for translational speeds of small oligonucleotides due to diffusion. In the region of the *y*-axis, however, within 5−8 μm of the wire surface, the velocity magnitudes are indeed well below 50 μm/s, and the temperature difference over that region is about 4 K.

In order to consider the Soret effect using the mathematical models provided by the Onsager relations in the linear formalism, a pressure gradient and the influence of viscous forces must not be involved.[54,55,59] When buoyancy forces are present in the system, the exact solution of the steady-state problem becomes much more difficult.[59] The linear model can

DOI: 10.1021/acsami.5b04435
ACS Appl. Mater. Interfaces 2015, 7, 19948−19959

possibly be applied locally, in the lower-velocity region near the wire. For this regime, the net effects of the thermophoretic force are observed after steady-state is reached between thermophoretic motion, and the subsequent concentration-gradient induced diffusive motion in the reverse direction in response to thermophoresis. Concentrations of DNA at the wire surface may also be affected by depletion by probe capture, as well as by influx of molecules from the more rapidly circulating bulk solution. An estimate for the time to reach steady state, also called the relaxation time, has been modeled by the equation $\tau = a^2/D\pi^2$, where a is the distance between the hot region and the cold region, and D is the ordinary diffusion coefficient. Using a value of 100 $\mu m^2/s$ for D, and a distance of 10 μm, the relaxation time may be a mere 100 ms. If changes to the concentration at the surface due to capture are balanced by influx from the bulk due to convective mixing, within 100−200 ms the required conditions may be achieved to predict a concentration gradient, in this local, quiescent region, due to the Soret effect.

For most systems in aqueous solution, the expected concentration enrichment at temperatures above 20 °C for the larger molecule in a solution (here the DNA) occurs at the cold side.[54,55,59] For DNA at room temperature, a difference of 2 K was sufficient for significant enrichment at the colder region.[58] According to our simulation results, a 2 K difference is found 5 μm from the wire surface at steady state, and a difference of 5 K is found within 15 μm from the wire surface. These conditions indicate a distinct possibility for a positive Soret effect driving unbound DNA away from the tethered probes. Furthermore, a local "thermophoretic force" driving DNA molecules away from a small hot region in solution in real time, not at steady state, has been observed both in laser-heated microfluidics experiments[61] and in atomic-level nonequilibrium molecular dynamics simulations.[60] Therefore, even without conditions approximating the steady state, this local thermophoretic force may begin driving DNA molecules away from the wire surface even during the first few microseconds of the experiment. In addition, the driving of DNA away from the heated wire may also help to drive the kinetics of the hybridization reaction, as the protective strand "products" after hybridization may also be driven away from the reaction site by thermophoresis. This helps to explain the decrease in optimum temperature found in the wire experiments as compared to those at the disc.

For the disc electrode system, the electrode, at room temperature, is dipped into a heated solution. For the first few seconds, it is possible that the reverse temperature gradient is found near the reaction surface. This situation would suggest a movement of DNA toward the tethered probes, at least until the disc reaches the temperature of the solution. Simulations of the disc experiment showed that such a temperature gradient does exist initially. Figure 9 shows temperature profiles along a line extending from the disc surface, at the solution interface, downward into the solution over 2 mm, for times of 3 to 11 s. Very small currents are also present, and do not completely settle until after 16 s (see the Supporting Information figures). The temperature gradients range from about 8 K to over 2 K for these times. Steady-state temperatures (a constant value over the entire system) are not reached until after 11−15 s. Thus, it is possible that thermodiffusion can occur in the first ten seconds, carrying DNA molecules toward the disc. This early stage enrichment at the electrode surface may contribute to increased initial capture. For later times, the absence of a temperature gradient (and a force driving DNA away from the electrode) may also explain some signal differences found in the experiments.

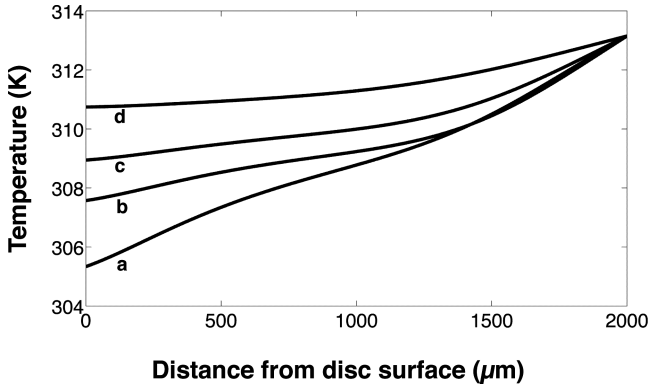

Figure 9. Temperature profiles along a line extending from disc surface into solution for time values of (a) 3 s, (b) 5 s, (c) 7 s, and (d) 11 s.

CONCLUSIONS

When optimizing the hybridization temperature for different maize DNA sequences, we found dramatic effects of DNA sequence upon the kinetics of strand displacement at gold electrodes in a heated hybridization solution, as well as directly heated gold wire electrodes. Three in four sequences revealed very high activation energy up to 200 kJ/mol during the hybridization step. We attribute this to the strand displacement of protective strands by the capture probes. These protective strands contained 4 to 5 mismatches to ease their displacement by the surface-confined capture probes at the gold electrodes. Sequence 810 revealed much lower activation energy (30−44 kJ/mol). This was attributed to a double mismatch at the end of the double-stranded part (a so-called toehold) besides two other mismatches. We found a similar hybridization behavior on directly heated gold wire electrodes as well. However, two major differences were observed: whereas the activation energy was significantly higher at the gold microwire, the optimal hybridization temperature was on average 23 K lower in comparison with the gold disk electrode in a heated bulk solution.

Considering the results for 810 as reporting on effects secondary to the strand-displacement step, it is possible to see some characteristics of these processes from the kinetics curves. A nonexponential shape and a reduced maximum value suggest the presence of multiple, equally influential parallel processes and the influence of sequence on these secondary processes, such as a possible reduced diffusion rate due to increased friction. Due to the steep temperature gradient around a heated gold microwire, we conclude that the Soret effect may potentially influence strand displacement kinetics at heated electrodes, through its effects on thermodiffusion of DNA. Further studies in this vein can attempt to differentiate the secondary processes in toehold-containing sequences by modifying, for instance, probe density and location of the osmium moiety. Future studies on DNA assays with surface-confined capture probes should take into consideration both possible thermodiffusive effects and sequence-specific variations in hybridization behavior. This applies, in particular, to assays that include a strand displacement step, such as competitive assays and molecular beacons. Analyses of surface-tethered molecular environments should also consider the potential influence of the Soret effect when any temperature gradients are expected to be present.

DOI: 10.1021/acsami.5b04435
ACS Appl. Mater. Interfaces 2015, 7, 19948−19959

■ ASSOCIATED CONTENT

Supporting Information

The Supporting Information is available free of charge on the ACS Publications website at DOI: 10.1021/acsami.5b04435.

Details on COMSOL simulations and error estimation of Arrhenius plots (PDF)

■ AUTHOR INFORMATION

Corresponding Author

*E-mail: gflechsig@albany.edu.

Notes

The authors declare the following competing financial interest(s): Gerd-Uwe Flechsig is a co-founder of Gensoric GmbH and holds more than 5% of its shares. Gensoric develops electrochemical instruments and biosensors and has delivered the HF ThermaLab heating generator used in this study.

■ ACKNOWLEDGMENTS

The authors are grateful for financial support: SUNY Albany start-up funds, German Federal Ministry for Economic Affairs and Energy (BMWi EXIST grant 03EGSMV040), as well as German Research Foundation (DFG Heisenberg Fellowship FL 384/7-2).

■ REFERENCES

(1) Campuzano, S.; Kuralay, F.; Lobo-Castañón, M. J.; Bartošík, M.; Vyavahare, K.; Paleček, E.; Haake, D. A.; Wang, J. Ternary Monolayers as DNA Recognition Interfaces for Direct and Sensitive Electrochemical Detection in Untreated Clinical Samples. *Biosens. Bioelectron.* **2011**, *26*, 3577−3583.

(2) Kuralay, F.; Campuzano, S.; Haake, D. A.; Wang, J. Highly Sensitive Disposable Nucleic Acid Biosensors for Direct Bioelectronic Detection in Raw Biological Samples. *Talanta* **2011**, *85*, 1330−1337.

(3) Mandler, D.; Kraus-Ophir, S. Self-Assembled Monolayers (SAMS) for Electrochemical Sensing. *J. Solid State Electrochem.* **2011**, *15*, 1535−1558.

(4) Wang, J.; Xu, D.; Kawde, A.-N.; Polsky, R. Metal Nanoparticle-Based Electrochemical Stripping Potentiometric Detection of DNA Hybridization. *Anal. Chem.* **2001**, *73*, 5576−5581.

(5) Ahour, F.; Pournaghi-Azar, M.; Hejazi, M. An Electrochemical Approach for Direct Detection and Discrimination of Fully Match and Single Base Mismatch Double-Stranded Oligonucleotides Corresponding to Universal Region of Hepatitis C Virus. *Anal. Methods* **2012**, *4*, 967−972.

(6) Bettazzi, F.; Lucarelli, F.; Palchetti, I.; Berti, F.; Marrazza, G.; Mascini, M. Disposable Electrochemical DNA-Array for PCR Amplified Detection of Hazelnut Allergens in Foodstuffs. *Anal. Chim. Acta* **2008**, *614*, 93−102.

(7) Paleček, E.; Bartosik, M. Electrochemistry of Nucleic Acids. *Chem. Rev.* **2012**, *112*, 3427−3481.

(8) Batchelor-McAuley, C.; Wildgoose, G. G.; Compton, R. G. The Physicochemical Aspects of DNA Sensing Using Electrochemical Methods. *Biosens. Bioelectron.* **2009**, *24*, 3183−3190.

(9) Jacobsen, M.; Flechsig, G.-U. Temperature Control in Electrochemical DNA Sensing. *Curr. Phys. Chem.* **2011**, *1*, 292−298.

(10) Bartosik, M.; Hrstka, R.; Palecek, E.; Vojtesek, B. Magnetic Bead-Based Hybridization Assay for Electrochemical Detection of microRNA. *Anal. Chim. Acta* **2014**, *813*, 35−40.

(11) Civit, L.; Fragoso, A.; O'Sullivan, C. K. Thermal Stability of Diazonium Derived and Thiol-Derived Layers on Gold for Application in Genosensors. *Electrochem. Commun.* **2010**, *12*, 1045−1048.

(12) Fiche, J.; Buhot, A.; Calemczuk, R.; Livache, T. Temperature Effects on DNA Chip Experiments From Surface Plasmon Resonance Imaging: Isotherms and Melting Curves. *Biophys. J.* **2007**, *92*, 935−946.

(13) Cisse, I. I.; Kim, H.; Ha, T. A Rule of Seven in Watson-Crick Base-Pairing of Mismatched Sequences. *Nat. Struct. Mol. Biol.* **2012**, *19*, 623−627.

(14) Pesciotta, E. N.; Bornhop, D. J.; Flowers, R., 2nd Back-Scattering Interferometry: A Versatile Platform for the Study of Free-Solution Versus Surface-Immobilized Hybridization. *Chem. - Asian J.* **2011**, *6*, 70.

(15) Johnson, R. P.; Gao, R.; Brown, T.; Bartlett, P. N. The Effect of Base-Pair Sequence on Electrochemically Driven Denaturation. *Bioelectrochemistry* **2012**, *85*, 7−13.

(16) Johnson, R. P.; Gale, N.; Richardson, J. A.; Brown, T.; Bartlett, P. N. Denaturation of dsDNA Immobilised at a Negatively Charged Gold Electrode Is Not Caused by Electrostatic Repulsion. *Chem. Sci.* **2013**, *4*, 1625−1632.

(17) Fan, C.; Plaxco, K. W.; Heeger, A. J. Electrochemical Interrogation of Conformational Changes as a Reagentless Method for the Sequence-Specific Detection of DNA. *Proc. Natl. Acad. Sci. U. S. A.* **2003**, *100*, 9134−9137.

(18) Ricci, F.; Lai, R. Y.; Heeger, A. J.; Plaxco, K. W.; Sumner, J. J. Effect of Molecular Crowding on the Response of an Electrochemical DNA Sensor. *Langmuir* **2007**, *23*, 6827−6834.

(19) Peterson, A. W.; Wolf, L. K.; Georgiadis, R. M. Hybridization of Mismatched or Partially Matched DNA at Surfaces. *J. Am. Chem. Soc.* **2002**, *124*, 14601−14607.

(20) Du, H.; Strohsahl, C. M.; Camera, J.; Miller, B. L.; Krauss, T. D. Sensitivity and Specificity of Metal Surface-Immobilized Molecular Beacon Biosensors. *J. Am. Chem. Soc.* **2005**, *127*, 7932−7940.

(21) Yang, A. H.; Hsieh, K.; Patterson, A. S.; Ferguson, B. S.; Eisenstein, M.; Plaxco, K. W.; Soh, H. T. Accurate Zygote-Specific Discrimination of Single-Nucleotide Polymorphisms Using Microfluidic Electrochemical DNA Melting Curves. *Angew. Chem.* **2014**, *126*, 3227−3231.

(22) Liepold, P.; Kratzmüller, T.; Persike, N.; Bandilla, M.; Hinz, M.; Wieder, H.; Hillebrandt, H.; Ferrer, E.; Hartwich, G. Electrically Detected Displacement Assay (Edda): A Practical Approach to Nucleic Acid Testing in Clinical or Medical Diagnosis. *Anal. Bioanal. Chem.* **2008**, *391*, 1759−1772.

(23) Surkus, A.-E.; Flechsig, G.-U. Electrochemical Detection of DNA Melting Curves by Means of Heated Biosensors. *Electroanalysis* **2009**, *21*, 1119−1123.

(24) Nasef, H.; Beni, V.; O'Sullivan, C. K. Electrochemical Melting-Curve Analysis. *Electrochem. Commun.* **2010**, *12*, 1030−1033.

(25) Nasef, H.; Beni, V.; O'Sullivan, C. K. Labelless Electrochemical Melting Curve Analysis for Rapid Mutation Detection. *Anal. Methods* **2010**, *2*, 1461−1466.

(26) Nasef, H.; Ozalp, V. C.; Beni, V.; OSullivan, C. K. Melting Temperature of Surface-Tethered DNA. *Anal. Biochem.* **2010**, *406*, 34−40.

(27) Belozerova, I.; Ge, D.; Levicky, R. *Nanomaterial Interfaces in Biology*; Springer: 2013; pp 127−136.

(28) Shen, Z.; Sintim, H. O.; Semancik, S. Rapid Nucleic Acid Melting Analyses Using a Microfabricated Electrochemical Platform. *Anal. Chim. Acta* **2015**, *853*, 265−270.

(29) Paleček, E.; Hung, M. A. Determination of Nanogram Quantities of Osmium-Labeled Nucleic Acids by Stripping (Inverse) Voltammetry. *Anal. Biochem.* **1983**, *132*, 236−242.

(30) Paleček, E. Probing of DNA Structure in Cells With Osmium Tetroxide-2, 2′-Bipyridine. *Methods Enzymol.* **1992**, *212*, 305.

(31) Flechsig, G.-U.; Reske, T. Electrochemical Detection of DNA Hybridization by Means of Osmium Tetroxide Complexes and Protective Oligonucleotides. *Anal. Chem.* **2007**, *79*, 2125−2130.

(32) Mix, M.; Reske, T.; Duwensee, H.; Flechsig, G.-U. Electrochemical Detection of Asymmetric PCR Products by Labeling With Osmium Tetroxide. *Electroanalysis* **2009**, *21*, 826−830.

(33) Paleček, E.; Trefulka, M.; Fojta, M. End-Labeling of Peptide Nucleic Acid With Osmium Complex. Voltammetry at Carbon and Mercury Electrodes. *Electrochem. Commun.* **2009**, *11*, 359−362.

(34) Fojta, M.; Kostečka, P.; Pivonkova, H.; Horakova, P.; Havran, L. Osmium Tetroxide Complexes as Versatile Tools for Structure Probing

DOI: 10.1021/acsami.5b04435
ACS Appl. Mater. Interfaces 2015, 7, 19948−19959

and Electrochemical Analysis of Biopolymers. *Curr. Anal. Chem.* **2011**, *7*, 35−50.
(35) Kostečka, P.; Havran, L.; Bittová, M.; Pivoňková, H.; Fojta, M. Sensing Mispaired Thymines in DNA Heteroduplexes Using an Electroactive Osmium Marker: Towards Electrochemical SNP Probing. *Anal. Bioanal. Chem.* **2011**, *400*, 197−204.
(36) Fojta, M.; Kostečka, P.; Trefulka, M.; Havran, L.; Palecek, E. Multicolor Electrochemical Labeling of DNA Hybridization Probes With Osmium Tetroxide Complexes. *Anal. Chem.* **2007**, *79*, 1022−1029.
(37) Duwensee, H.; Mix, M.; Broer, I.; Flechsig, G.-U. Electrochemical Detection of Modified Maize Gene Sequences by Multiplexed Labeling with Osmium Tetroxide Bipyridine. *Electrochem. Commun.* **2009**, *11*, 1487−1491.
(38) Mix, M.; Rüger, J.; Krüger, S.; Broer, I.; Flechsig, G.-U. Electrochemical Detection of 0.6% Genetically Modified Maize MON810 in Real Flour Samples. *Electrochem. Commun.* **2012**, *22*, 137−140.
(39) Liu, R. H.; Lenigk, R.; Druyor-Sanchez, R. L.; Yang, J.; Grodzinski, P. Hybridization Enhancement Using Cavitation Microstreaming. *Anal. Chem.* **2003**, *75*, 1911−1917.
(40) Sosnowski, R. G.; Tu, E.; Butler, W. F.; OConnell, J. P.; Heller, M. J. Rapid Determination of Single Base Mismatch Mutations in DNA Hybrids by Direct Electric Field Control. *Proc. Natl. Acad. Sci. U. S. A.* **1997**, *94*, 1119−1123.
(41) Flechsig, G.-U.; Peter, J.; Hartwich, G.; Wang, J.; Gründler, P. DNA Hybridization Detection at Heated Electrodes. *Langmuir* **2005**, *21*, 7848−7853.
(42) Zerihun, T.; Gründler, P. Electrically Heated Cylindrical Microelectrodes. Determination of Lead on Pt by Cyclic Voltammetry and Cathodic Stripping Analysis. *J. Electroanal. Chem.* **1996**, *415*, 85−88.
(43) Flechsig, G.-U.; Korbout, O.; Hocevar, S. B.; Thongngamdee, S.; Ogorevc, B.; Gründler, P.; Wang, J. Electrically Heated Bismuth-Film Electrode for Voltammetric Stripping Measurements of Trace Metals. *Electroanalysis* **2002**, *14*, 192−196.
(44) Wang, J.; Gründler, P.; Flechsig, G.-U.; Jasinski, M.; Rivas, G.; Sahlin, E.; Lopez Paz, J. L. Stripping Analysis of Nucleic Acids at a Heated Carbon Paste Electrode. *Anal. Chem.* **2000**, *72*, 3752−3756.
(45) Gründler, P.; Flechsig, G.-U. Principles and Analytical Applications of Heated Electrodes. *Microchim. Acta* **2006**, *154*, 175−189.
(46) Gründler, P.; Kirbs, A.; Dunsch, L. Modern Thermoelectrochemistry. *ChemPhysChem* **2009**, *10*, 1722−1746.
(47) Flechsig, G.-U.; Walter, A. Electrically Heated Electrodes: Practical Aspects and New Developments. *Electroanalysis* **2012**, *24*, 23−31.
(48) Gründler, P. *In-Situ Thermoelectrochemistry: Working With Heated Electrodes*; Springer: 2015.
(49) Wachholz, F.; Gimsa, J.; Duwensee, H.; Grabow, H.; Gründler, P.; Flechsig, G.-U. A Compact and Versatile Instrument for Radio Frequency Heating in Nonisothermal Electrochemical Studies. *Electroanalysis* **2007**, *19*, 535−540.
(50) Hilaire, M. R.; Abaskharon, R. M.; Gai, F. Biomolecular Crowding Arising From Small Molecules, Molecular Constraints, Surface Packing, and Nano-Confinement. *J. Phys. Chem. Lett.* **2015**, *6*, 2546−2553.
(51) Rao, A. N.; Grainger, D. W. Biophysical Properties of Nucleic Acids at Surfaces Relevant to Microarray Performance. *Biomater. Sci.* **2014**, *2*, 436−471.
(52) Watkins, H. M.; Simon, A. J.; Ricci, F.; Plaxco, K. W. Effects of Crowding on the Stability of a Surface-Tethered Biopolymer: An Experimental Study of Folding in a Highly Crowded Regime. *J. Am. Chem. Soc.* **2014**, *136*, 8923−8927.
(53) Nkoua Ngavouka, M. D.; Bosco, A.; Casalis, L.; Parisse, P. Determination of Average Internucleotide Distance in Variable Density ssDNA Nanobrushes in the Presence of Different Cations Species. *Macromolecules* **2014**, *47*, 8748−8753.
(54) Platten, J. K. The Soret Effect: A Review of Recent Experimental Results. *J. Appl. Mech.* **2006**, *73*, 5−15.
(55) Mazur, P.; de Groot, S. R. *Non-Equilibrium Thermodynamics*; North-Holland: 1963.
(56) Wiegand, S. In *Experimental Thermodynamics Vol. IX: Advances in Transport Properties of Fluids*; Assael, M. J., Goodwin, A. R. H., Vesovic, V., Wakeham, W. A., Eds.; Experimental Thermodynamics Series; Royal Society of Chemistry: Cambridge, UK, 2014.
(57) Yu, L.-H.; Chen, Y.-F. Concentration-Dependent Thermophoretic Accumulation for the Detection of DNA Using DNA-Functionalized Nanoparticles. *Anal. Chem.* **2015**, *87*, 2845−2851.
(58) Duhr, S.; Braun, D. Why Molecules Move Along a Temperature Gradient. Proc. *Proc. Natl. Acad. Sci. U. S. A.* **2006**, *103*, 19678−19682.
(59) Andreev, V. K.; Gaponenko, Y. A.; Goncharova, O. N.; Pukhnachev, V. V. *Mathematical Models of Convection*; Walter de Gruyter: 2012; Vol. *5*.
(60) Belkin, M.; Chao, S.-H.; Giannetti, G.; Aksimentiev, A. Modeling Thermophoretic Effects in Solid-State Nanopores. *J. Comput. Electron.* **2014**, *13*, 826−838.
(61) Thamdrup, L. H.; Larsen, N. B.; Kristensen, A. Light-Induced Local Heating for Thermophoretic Manipulation of DNA in Polymer Micro-and Nanochannels. *Nano Lett.* **2010**, *10*, 826−832.
(62) Reineck, P.; Wienken, C. J.; Braun, D. Thermophoresis of Single Stranded DNA. *Electrophoresis* **2010**, *31*, 279−286.
(63) Sopha, H.; Wachholz, F.; Flechsig, G.-U. Cathodic Adsorptive Stripping Voltammetric Detection of tRNA by Labelling With Osmium Tetroxide. *Electrochem. Commun.* **2008**, *10*, 1614−1616.
(64) Zhang, D. Y.; Seelig, G. Dynamic DNA Nanotechnology Using Strand-Displacement Reactions. *Nat. Chem.* **2011**, *3*, 103−113.
(65) Zhang, D. Y.; Winfree, E. Control of DNA Strand Displacement Kinetics Using Toehold Exchange. *J. Am. Chem. Soc.* **2009**, *131*, 17303−17314.
(66) Flechsig, G.-U.; Reske, T. Method for Labelling and Analysing Nucleic Acids. 2005; Patent, DE 10 2005 039 726, US 8,216,446.
(67) Urakawa, H.; Noble, P. A.; el Fantroussi, S.; Kelly, J. J.; Stahl, D. A. Single-Base-Pair Discrimination of Terminal Mismatches by Using Oligonucleotide Microarrays and Neural Network Analyses. *Appl. Environ. Microbiol.* **2002**, *68*, 235−244.
(68) Peter, J.; Reske, T.; Flechsig, G.-U. Comparison of DNA Hybridization at Rotating and Heated Gold Disk Electrodes. *Electroanalysis* **2007**, *19*, 1356−1361.
(69) Flechsig, G.-U.; Korbut, O.; Gründler, P. Investigation of Deposition and Stripping Phenomena at the Heated Gold Wire Electrode in Comparison to the Rotating Disk Electrode: Copper (II), Mercury (II), and Arsenic (III). *Electroanalysis* **2001**, *13*, 786−788.
(70) Engelhardt, G.; Lvov, S.; Macdonald, D. Importance of Thermal Diffusion in High Temperature Electrochemical Cells. *J. Electroanal. Chem.* **1997**, *429*, 193−201.
(71) Beckmann, A.; Coles, B. A.; Compton, R. G.; Gründler, P.; Marken, F.; Neudeck, A. Modeling Hot Wire Electrochemistry. Coupled Heat and Mass Transport at a Directly and Continuously Heated Wire. *J. Phys. Chem. B* **2000**, *104*, 764−769.
(72) Reichl, M.; Herzog, M.; Götz, A.; Braun, D. Why Charged Molecules Move Across a Temperature Gradient: The Role of Electric Fields. *Phys. Rev. Lett.* **2014**, *112*, 198101.
(73) Gründler, P. Phenomena at Hot-Wire Electrodes. *Fresenius' J. Anal. Chem.* **2000**, *367*, 324−328.
(74) Lapham, J.; Rife, J. P.; Moore, P. B.; Crothers, D. M. Measurement of Diffusion Constants for Nucleic Acids by NMR. *J. Biomol. NMR* **1997**, *10*, 255−262.

DOI: 10.1021/acsami.5b04435
ACS Appl. Mater. Interfaces 2015, 7, 19948−19959